European Journal of Radiology Open 14 (2025) 100651

Contents lists available at ScienceDirect

European Journal of Radiology Open

journal homepage: www.elsevier.com/locate/ejro

Radiomics in differential diagnosis of pancreatic tumors

Riccardo De Robertis [a], Beatrice Mascarin [b,*], Eda Bardhi [b], Flavio Spoto [b], Nicolò Cardobi [a], Mirko D'Onofrio [a]

[a] Department of Radiology, G.B. Rossi Hospital, University of Verona, Piazzale L.A. Scuro 10, Verona 37134, Italy
[b] Department of Radiology, University of Verona, Verona, Italy

ARTICLE INFO

Keywords:
Radiomics
Pancreatic Tumors
Texture Analysis
Contrast-Enhanced CT Scans
Pancreatic Ductal Adenocarcinoma
Pancreatic Neuroendocrine Tumors

ABSTRACT

The aim of this study was to assess whether radiomics could predict histotype of pancreatic ductal adenocarcinomas (PDAC) and pancreatic neuroendocrine tumors (PNET). Contrast-enhanced CT scans of 193 patients were retrospectively reviewed, encompassing 97 PDACs and 96 PNETs. Additionally, anamnestic data and laboratory data were evaluated. A total of 107 features were extracted for both the arterial and venous phases. ROC curves were constructed for the parameters with the highest AUC, considering two groups: one including all lesions and the other including only lesions smaller than 5 cm. The following feature differences were found to be statistically significant ($p < 0.05$). Without considering lesion size: for the arterial phase, 16 first-order and 38 s-order features; for the venous phase, 10 first-order and 20 s-order features. When considering lesion size: for the arterial phase, 16 first-order and 52 s-order features; for the venous phase, 11 first-order and 36 s-order features. The radiomics features with the highest AUC values included ART_firstorder_RootMeanSquared (AUC = 0.896, $p < 0.01$) in the arterial phase and VEN_firstorder_Median (AUC = 0.737, $p < 0.05$) in the venous phase for all lesions, and ART_firstorder_RootMeanSquared (AUC = 0.859, $p < 0.01$) and VEN_firstorder_Median (AUC = 0.713, $p < 0.05$) for lesions smaller than 5 cm. Texture analysis of pancreatic pathology has shown good predictability in defining the PNET histotype. This analysis potentially offering a non-invasive, imaging-based method to accurately differentiate between pancreatic tumor types. Such advancements could lead to more precise and personalized treatment planning, ultimately optimizing the use of medical resources.

1. Introduction

Diagnosing pancreatic lesions, such as Pancreatic Ductal Adenocarcinoma (PDAC) and pancreatic neuroendocrine tumor (PNET), relies on a multidisciplinary approach, integrating clinical suspicion with biochemical and imaging assessments. Definitive diagnosis, however, requires histological confirmation via core-needle biopsy or surgical specimens for resectable tumors [1].

PDAC the most prevalent pancreatic tumor, is notorious for its high aggressiveness and mortality. Its poor prognosis stems from often asymptomatic early stages and aggressive tumor biology [2]. Diagnostic evaluation involves serum biomarkers (CA 19–9, CEA), advanced imaging, and for borderline resectable and advanced PDAC also the biopsy [3]. Typically, PDAC at imaging presents as hypodense masses with indistinct margins. Early detection remains challenging, but comprehensive imaging facilitates timely diagnosis, revealing mass effects like parenchymal atrophy and the "duct-interrupted sign".

PNETs include a heterogeneous group of rare neoplasms, distinguished into functioning and non-functioning types based on hormone secretion. Imaging, particularly CT and MRI, plays a crucial role in their loco-regional evaluation. PNETs tend to be hypervascular and well-circumscribed, with small tumors (<2 cm) appearing homogenous and larger masses presenting heterogeneously [4]. This diversity complicates differential diagnosis with PDAC, underscoring the limitations of relying solely on contrast enhancement for mass evaluation.

Radiomics involves the extraction of quantitative and reproducible data from radiological images. These data reflect the tissue heterogeneity, potentially having immediate implications in clinic. Collected extensively and analyzed through artificial intelligence programs [5], radiomic data can form the basis for studying new biomarkers [6]. Unlike the traditional qualitative analysis in clinical practice, radiomics leverages a vast amount of objective data, extracted from images, providing insights into dimensions, shape, and structural features. This allows for the creation of statistical models to support diagnosis [7]. The

* Corresponding author.
E-mail address: beatrice.mascarin@gmail.com (B. Mascarin).

https://doi.org/10.1016/j.ejro.2025.100651
Received 26 July 2024; Received in revised form 27 March 2025; Accepted 6 April 2025
Available online 6 May 2025
2352-0477/© 2025 Published by Elsevier Ltd. This is an open access article under the CC BY-NC-ND license (http://creativecommons.org/licenses/by-nc-nd/4.0/).

grayscale values in these images, and their spatial and temporal relationships, reveal phenotypic variations within the lesion, indicative of underlying genetic and molecular differences [6]. Radiomics is applicable across various imaging techniques, including CT and MRI. Texture analysis, a branch of radiomics, quantitatively and qualitatively assesses gray-scale variations, spatial relationships, and pixel/voxel distribution within a region of interest (ROI) [8]. This approach offers valuable spatial information about the lesion, using both predefined features and "deep features" from machine learning algorithms. A typical radiomic analysis involves image acquisition, segmentation, feature extraction, and statistical analysis [6]. Despite the challenges in standardizing image acquisition protocols across different platforms, radiomics aims to build models applicable to diverse imaging protocols. Segmenting the ROI can be manual or automated. Radiomics features are divided into first-order, second-order, and higher-order categories, with first-order features and higher-order features [5].

First-order features are derived from the histogram representing the overall gray-level distribution within ROI denoted by Hounsfield units. These features include statistical descriptors such as mean, minimum, maximum, variance, percentiles, skewness, kurtosis, entropy, and uniformity [9]. Entropy measures the randomness in gray-level distribution, increasing with more random distributions, while uniformity does the opposite. Skewness indicates the asymmetry of the data distribution curve, either left-skewed (below the mean) or right-skewed (above the mean). Kurtosis assesses the deviation from a normal Gaussian distribution, indicating either a flatter or more peaked curve.

Second-order features summarize the local spatial arrangement of intensities between two pixels/voxels within the ROI [10]. Higher-order features analyze the relationships among three or more pixels/voxels. The Gray-Level Co-occurrence Matrix (GLCM) assesses spatial relationships between voxel pairs with specific gray levels in various directions and distances, including entropy, angular moment (or energy/uniformity), and contrast. The Gray-Level Run-Length Matrix (GLRLM) provides information about the spatial distribution of voxels aligned with the same gray level in one or more directions, with features such as gray-level and run-length nonuniformity evaluating gray level distribution and run length. The Gray-Level Zone-Length Matrix (GLZLM) examines clusters of adjacent voxels (zones) with the same gray intensity. The Neighborhood Gray-Tone Difference Matrix (NGTDM) quantifies differences between a voxel's gray level and the mean gray level of its neighboring voxels within a defined distance, describing coarseness, busyness, and complexity. The Neighborhood Gray-Level Difference Matrix (NGLDM) studies the spatial relationship of gray levels between a central voxel and its neighbors, considering proximity and gray-level differences. Examples of higher-order features include contrast (local variation within the image) and busyness (spatial rate of gray-level changes).

In pancreatic diagnostics, radiomic analysis shows promise for characterizing lesions, assessing treatment responses, and guiding prognosis, although further standardization and correlation with pathological data are needed to enhance its clinical utility [11].

In 2021 Chen et al.l. published the first study that showed that radiomics could distinguish pancreatic cancer from normal pancreas [12]. Consequently, the aim of this study was to evaluate whether radiomics, through the analysis of the features obtained from the texture analysis of different pancreatic tumors, was able to predict the histotype; in particular, PDAC and PNET were compared.

2. Materials and methods

2.1. Study population

During the recruitment phase, conducted retrospectively, a total of 213 patients, 108 with PDAC and 105 patients with PNET tumors were identified. The diagnosis was confirmed through histological results obtained from biopsy or, when available, from surgical specimens. Inclusion and exclusion criteria were established for patient enrollment in the study. The inclusion criteria included: the presence of CT images with iodinated contrast medium, histological confirmation of the tumor type, and the presence of primary lesions that had not undergone chemotherapy or radiotherapy. Exclusion criteria included: low-quality images or the presence of major artifacts (e.g., beam hardening from metallic prostheses), lesions that had already undergone chemotherapy, radiotherapy, or surgery. Clinical and anamnestic data related to pancreatic disease were also evaluated, such as the tumor marker CA19–9, the presence or new onset of diabetes, smoking habits, the appearance of jaundice, and the treatment performed (surgery, chemotherapy, or radiotherapy). Additionally, where possible, the tumor stage of adenocarcinomas, the grade, and functionality of PNETs (assessing the secretion of insulin, C-peptide, gastrin, alpha-fetoprotein, and serotonin) were recorded.

2.2. CT protocols and image acquisition

The patients in this study underwent preoperative abdominal contrast-enhanced CT scans over with both arterial and venous phase. CE-CT scans were performed at our institution (GB Rossi University Hospital) on CT scanner: - PHILIPS BRILLIANCE 64 slice CT scanner. The scanning voltage ranged from 100 kVp to 120 kVp, 125–250 mAs, pitch= 1. Images in the pancreatic parenchymal and portal venous phases were reconstructed at (2.0 mm) slice thickness. Images were acquired intravenously after injecting iodine-containing contrast media. Bolus tracking was used, the late arterial/pancreatic parenchymal phase was obtained approximately 40–45 s after the start of contrast injection, and an additional 20 s delay, a portal venous phase, was obtained approximately 65–70 s after the start of contrast injection.

2.3. Radiomic segmentation

The segmentation process was performed using 3D Slicer version 5.4, an open-source software application designed for medical image computing and visualization. A radiology resident, segmented the 3D tumor volumes of interest (VOI) for each patient. After this step, the segmentations were reviewed by an expert abdominal radiologist with over 10 years of experience. For all patients with PDAC and PNET, only the primary pancreatic lesion was segmented. Both the arterial and portal venous phases were utilized for segmentation for each subject. Tumors were delineated on axial, coronal, and sagittal planes. To address potential variability in image characteristics due to differing scanning parameters (e.g., tube voltage ranging from 100 kVp to 120 kVp and current-time settings from 125–250 mAs), image harmonization techniques, such as intensity normalization, were applied prior to feature extraction. The training and test sets were created using a random split of 70 % for training and 30 % for testing, with cross-validation to assess model performance. The radiomics features extracted adhered to the Image Biomarker Standardization Initiative (IBSI) framework [13], ensuring consistency and reproducibility. A total of 120 texture features were extracted using a PyRadiomics an open-source python package for the extraction of Radiomics features from medical imaging and including: First Order Statistics (19 features), Shape-based (3D) (16 features), Shape-based (2D) (10 features), Gray Level Co-occurrence Matrix (24 features), Gray Level Run Length Matrix (16 features), Gray Level Size Zone Matrix (16 features), Neighbouring Gray Tone Difference Matrix (5 features), Gray Level Dependence Matrix (14 features).

2.4. Statistical analysis

Nominal and ordinal variables are reported as percentage frequencies. Continuous variables with a Gaussian distribution are presented as mean ± standard deviation, while continuous variables with a non-normal distribution are reported as median [interquartile range].

The Kolmogorov-Smirnov test was used to assess the normality of the sample distributions. For group comparisons, the Mann-Whitney test for multiple independent samples was utilized. For each texture parameter that was significant, p-values < 0.05 were considered significant. Significant parameters derived from the histogram were tested using ROC curves, and parameters with the best AUC were extracted. The confidence interval was set at 95 %. Statistical analysis was conducted using IBM SPSS Statistics v20.0 (IBM, Chicago, USA) for Microsoft Windows.

To assess the agreement between the radiomic data and the radiologist's report, the McNemar test was employed.

3. Results

3.1. Population study

After applying inclusion and exclusion criteria, the final cohort retrospectively included in the study consisted of 193 patients. This cohort comprised 97 patients with PDAC and 96 patients with PNET. The study population included 101 males and 92 females, with a mean age of 52 ± 34 years. Anamnestic and clinical data were also evaluated (Table 1).

A secondary analysis was conducted, excluding lesions larger than 5 cm because PNET are generally larger, and including lesions of greater size could introduce bias by increasing the likelihood of classifying the lesion as PNET; for this purpose, we identified 86 patients with PDAC and 57 patients with PNET.

The average dimensions of pancreatic lesions in PDAC and PNET, based on their location within the pancreas, are presented in Table 2.

3.2. Radiomic segmentation

Segmentation was possible in all tumors. The Regions Of Interest (ROI) were drawn manually on the CT images tracing slice-by-slice the margin of the mass, taking care to avoid any arterial and venous vessels, surrounding adipose tissue or normal pancreatic tissue so to obtain a 3D volume of the lesion.

Once the tumor segmentations in both phases were concluded, radiomic data were extracted.

Examples of segmentation are presented in the Figs. 1 and 2.

3.3. Texture analysis

107 features were extracted from each arterial and venous phase.

Considering both the two groups, 85 differences in features were found with significant results (Fig. 3):

- in the arterial phase a total of 54 features with $p < 0.05$ of which 16 first order and 38 second order.
- in the venous phase a total of 31 features with $p < 0.05$ of which 10 are first order and 20 second order.

Considering instead, lesions smaller than 5 cm, 139 differences in features were found with significant results (Fig. 4):

Table 1
Clinical and anamnestic characteristics of the study population, comparing patients with PDAC and PNET.

	PDAC (n = 97)	PNET (n = 96)
Male	49	52
Age (years)	63 ± 23	52 ± 34
Smoke (%)	38	23
Diabetes (%)	18	12
Jaundice (%)	29	8
CA19–9 (U/ml)	1554,74	217,44

Table 2
Average lesion size and distribution within the pancreas (head, body, tail) for PDAC and PNET.

	PDAC	PNET
Average lesion size (mm)	30	43
Head	61	39
Body	25	34
Tail	11	23

- in the arterial phase a total of 80 features with $p < 0.05$ of which 16 first order.
- in the venous phase a total of 59 features with $p < 0.05$ of which 11 first order.

ROC curves were plotted and the respective areas under the curve (AUC) were calculated for the statistically significant results. Only the values having the best areas under the curve in predicting the neuroendocrine pathology with an interval of confidence set at 95 % were reported.

Without differentiating the dimensions of the lesions, the features with the best area under the curve in predicting neuroendocrine disease were:

ART_firstorder_10Percentile (AUC = 0.848),
ART_firstorder_90Percentile (AUC = 0.866),
ART_firstorder_Mean (AUC = 0.868),
ART_firstorder_Median (AUC = 0.866),
ART_firstorder_RootMeanSquared (AUC = 0.896),
VEN_firstorder_10Percentile (AUC = 0.715),
VEN_firstorder_90Percentile (AUC = 0.708),
VEN_firstorder_Mean (AUC = 0.734),
VEN_firstorder_Median (AUC = 0.737),
VEN_firstorder_RootMeanSquared (AUC = 0.736).

From the analysis of the ROC curves, it can be highlighted how the features relating to the arterial phase are more sensitive and specific than the venous phase in predicting PNETs. (Fig. 5)

For lesions smaller than 5 cm, the features with the best area under the curve in predicting neuroendocrine disease were:

ART_firstorder_10Percentile (AUC = 0.837),
ART_firstorder_90Percentile (AUC = 0.856),
ART_firstorder_Mean (AUC = 0.858),
ART_firstorder_Median (AUC = 0.856),
ART_firstorder_RootMeanSquared (ACU = 0.859),
VEN_firstorder_10Percentile (AUC = 0.694),
VEN_firstorder_90Percentile (AUC = 0.685),
VEN_firstorder_Mean (AUC = 0.71),
VEN_firstorder_Median (AUC = 0.713),
VEN_firstorder_RootMeanSquared (AUC = 0.712).

The analysis of the ROC curves between the statistically significant values, showed that Arterial features had greater predictability for PNETs than venous ones, proving to be more sensitive and specific. (Fig. 6)

The features with the best area under the curve in predicting neuroendocrine disease are summarized in the Table 3. The analysis of the ROC curves showed that the features relating to the arterial phase are more sensitive and specific than the venous ones in predicting neuroendocrine tumors.

To sum up, the p-values for the statistical comparisons of the radiomics features with the highest AUC were as follows: for ART_firstorder_RootMeanSquared (AUC = 0.896), $p < 0.01$; for VEN_firstorder_Median (AUC = 0.737), $p < 0.05$ in the all-lesion group; and for ART_firstorder_RootMeanSquared (AUC = 0.859), $p < 0.01$; for VEN_firstorder_Median (AUC = 0.713), $p < 0.05$ in the < 5 cm lesion group.

The data derived from radiomics and the radiologist's report were compared using the McNemar test, yielding a concordance rate of 0.815.

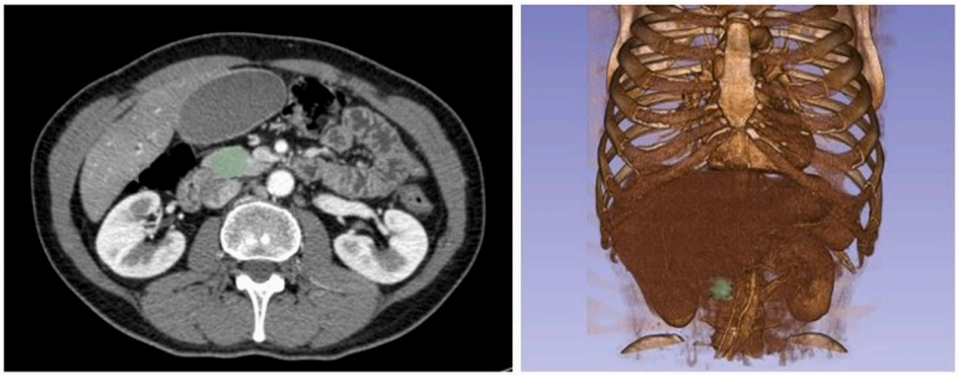

Fig. 1. Segmentation of a ductal adenocarcinoma involving the head of the pancreas. A: arterial phase with evidence of the lesion (green); B. 3D reconstruction of the lesion in the arterial phase (green).

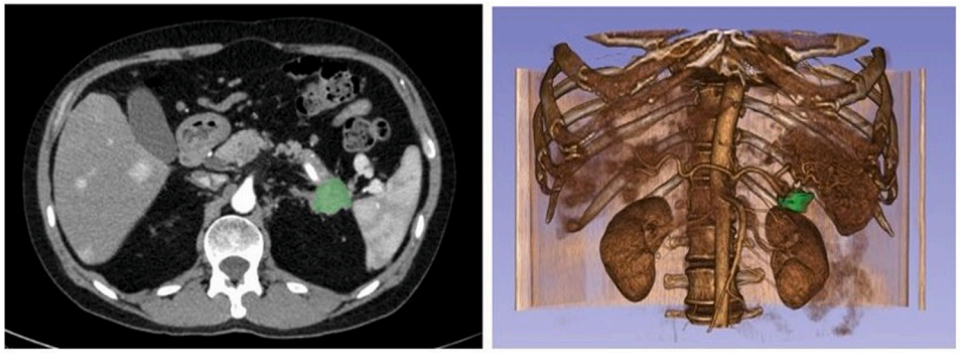

Fig. 2. Segmentation of a pancreatic neuroendocrine tumor involving the tail of the pancreas. A: arterial phase with evidence of the lesion (green); B. 3D reconstruction of the lesion in the arterial phase (green).

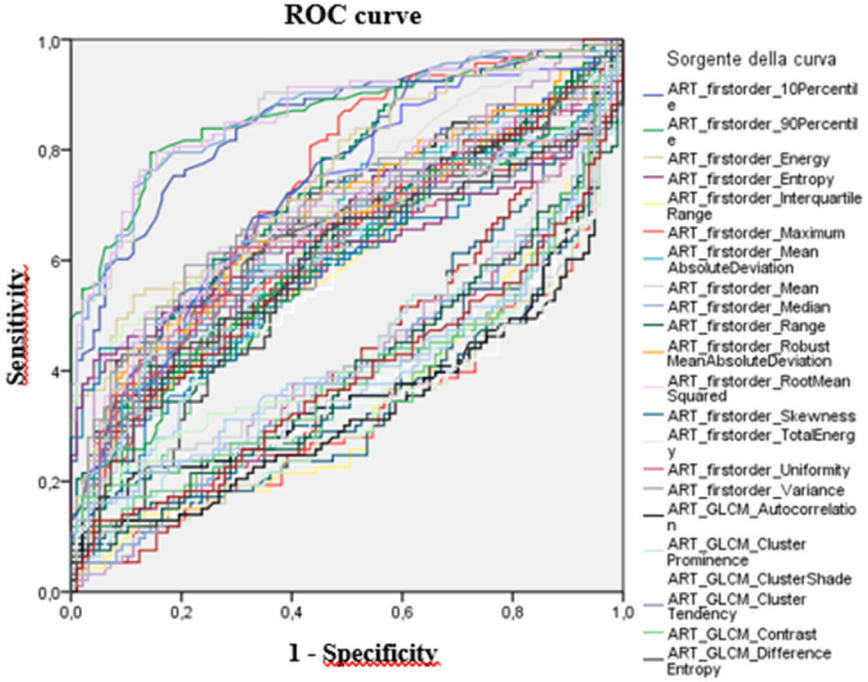

Fig. 3. ROC curves between the features resulting with a statistically significant difference ($p < 0.05$) from the comparison between the two groups in the prediction of neuroendocrine tumors.

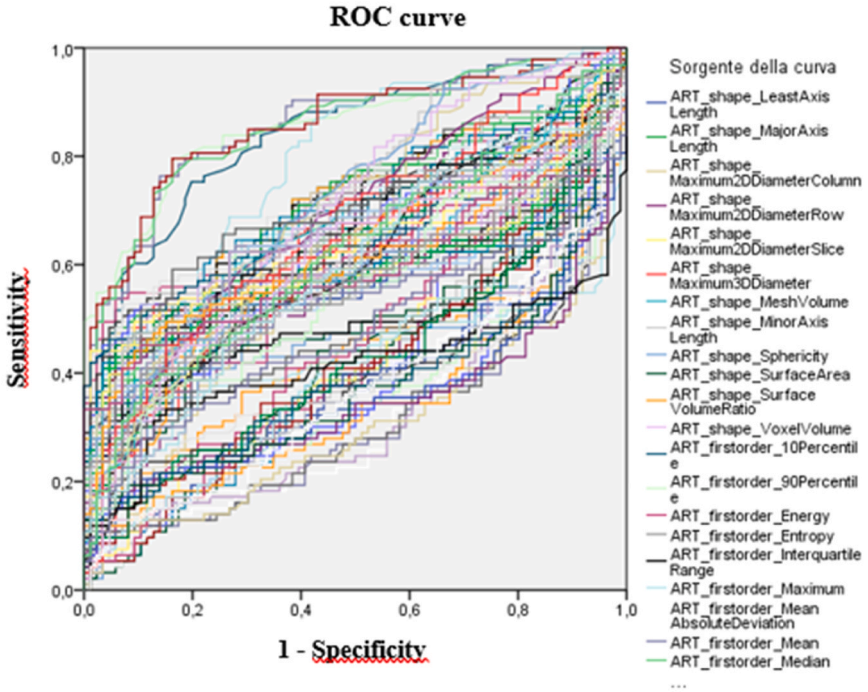

Fig. 4. ROC curves between the features resulting with a statistically significant difference ($p < 0.05$) from the comparison between the two groups with tumors measuring less than 5 cm in the prediction of neuroendocrine tumors.

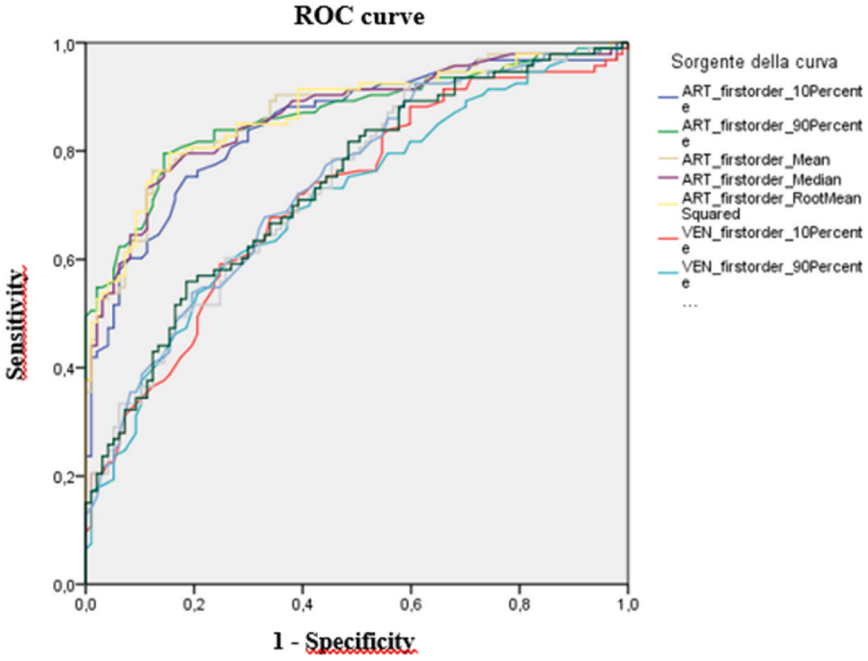

Fig. 5. ROC curves with the highest area under the curve (AUC) among the features resulting with a statistically significant difference ($p < 0.05$) from the comparison between the two groups in the prediction of neuroendocrine tumors.

4. Discussion

The aim of this study was to determine whether tumor histotype of pancreatic lesions, specifically PDAC and PNET, could be predicted through texture analysis and radiomics. This technique seeks to overcome the limitations of the "human eye" for detailed analysis of medical images by extracting characteristics known as radiomic features. Together, these features form what is known as a "radiomic signature." Another advantage of radiomic analysis is its almost negligible invasiveness, as it utilizes already available diagnostic images, and its low cost [9].

This field of research includes texture analysis, which can evaluate tissue heterogeneity by analyzing the distribution and relationship of gray levels in pixels or voxels in images. These can be used to predict histological types, assess treatment response, and estimate prognosis in various tumors, such as in non-small cell lung cancer [14], esophageal cancer [15], and colorectal cancer [16].

In the past decade, several authors have correlated imaging

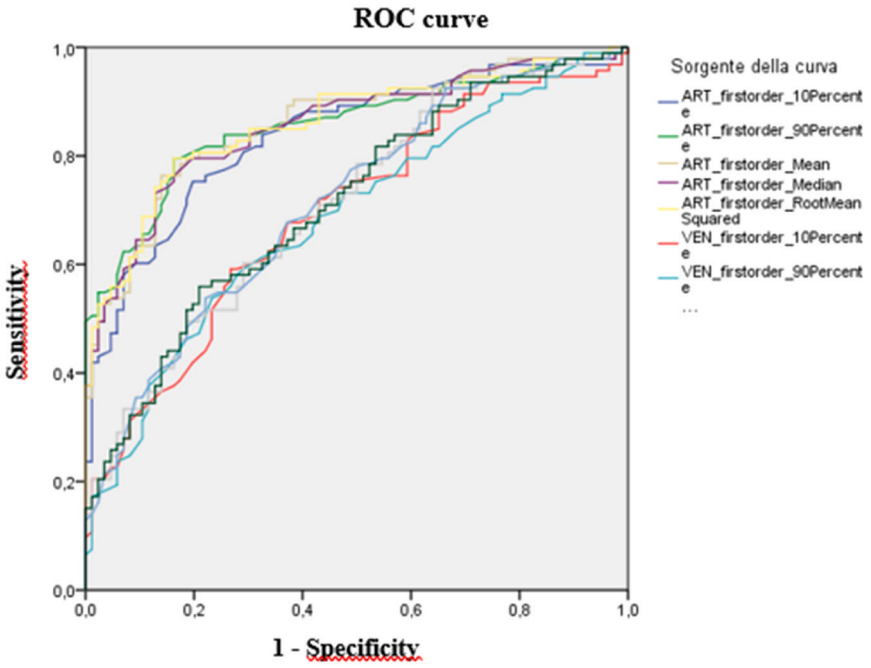

Fig. 6. ROC curves with the highest area under the curve (AUC) among the features resulting with a statistically significant difference ($p < 0.05$) from the comparison between the two groups in the prediction of neuroendocrine tumors considering lesions smaller than 5 cm.

Table 3
Radiomic features with the highest area under the curve (AUC) values for predicting PNET in lesions larger and smaller than 5 cm.

Features significative	AUC lesions > 5 cm	AUC lesions < 5 cm
ART_firstorder_10Percentile	0848	0837
ART_firstorder_90Percentile	0866	0856
ART_firstorder_Mean	0868	0858
ART_firstorder_Median	0866	0856
ART_firstorder_RootMeanSquared	0896	0859
VEN_firstorder_10Percentile	0715	0694
VEN_firstorder_90Percentile	0708	0685
VEN_firstorder_Mean	0734	0,71
VEN_firstorder_Median	0737	0713
VEN_firstorder_RootMeanSquared	0736	0712

characteristics with PDAC differentiation, prediction of lymph node or liver metastasis risk [17], treatment response, preoperative risk stratification, and their complications [18]. For instance, recently, using radiomic, it was demonstrated that metastatic PDAC had ill-defined margins, hypodense appearance, larger size, and lower arterial, perfusion, and permeability indices compared to non-metastatic PDAC [19].

As mentioned, for identify pathognomonic radiomic features for PDAC and PNET, a secondary analysis was performed excluding lesions larger than 5 cm [1].

The analysis comparing the two groups revealed statistically significant differences, with a larger area under the curve (AUC) for predicting PNET compared to PDAC, thus the study focused on predicting the former.

Certain radiomic features emerged as predictive for the diagnosis of PNET. It was observed that the group including lesions larger than 5 cm had higher AUC values compared to those with lesions smaller than 5 cm, reflecting the tendency of PNET to be more voluminous. Arterial features showed greater predictiveness for PNET compared to venous ones, proving to be more sensitive and specific in this phase. This phenomenon can be attributed to the hypervascular radiological phenotype typical of PNET, which often presents early enhancing in the arterial phase after contrast administration and slow washout in the venous phase, appearing as a hyperdense lesion against the remaining pancreatic parenchyma [4]. The arterial phase of post-contrast scanning particularly highlights small PNETs, which can be difficult to visualize in other phases. When they have an exophytic appearance and larger dimensions, they are better visualized in the venous phase [20]. Moreover, leveraging the contrastographic characteristics of panNETs in particular in the arterial phase, it was demonstrated that it could be predicted the grade of panNETs using qualitative and quantitative CT evaluation, and 3D CT-texture analysis [21].

First-order radiomic characteristics, which describe the distribution of voxel intensity within the ROI, were found to be more significant. Specifically, in contrast-enhanced CT, higher percentiles (75th and 90th) often reflect the blood perfusion of the lesion, while lower percentiles (5th and 10th) reflect cystic degeneration and necrosis. This study showed that the 10th and 90th percentiles in both arterial and venous phases are predictive for the diagnosis of PNET, reflecting the common finding of degenerative cysts within the tumors and their high vascularization.

Li J. et al. [22] analyzed CT images in the portal phase through radiomics, highlighting that the 10th percentile and skewness are significant features in differentiating PNET from PDAC (AUC = 0.848; 0.399 respectively). According to the results of Reinert C. et al. [23], some first-order characteristics obtained in our study proved relevant in predicting PNET diagnosis compared to PDAC, particularly the median (AUC = 0.866). Wang Z. et al. [24] evaluated the differential diagnosis specifically between PDAC and hypovascular PNET, emphasizing the role of the firstorder_RootMeanSquared feature, which was also statistically significant in our study in predicting PNET (AUC = 0.869). Other commonly considered characteristics for the quantitative evaluation of PNETs include entropy (degree of lesion heterogeneity), skewness (microenvironmental heterogeneity of the lesion), and kurtosis, which in this study did not emerge as predictive features (AUC = 0.603; 0.399; 0.671, respectively) [20]. This may be due to sample limitations and manual segmentation.

Regarding statistical analysis, the results of this study can be compared to those of Zhang T. et al. [25], which aimed to evaluate the diagnostic capability of radiomics combined with multiple machine learning algorithms to differentiate PDAC from PNET. Significant differences emerged among various parameters: higher levels of CA19–9 in

PDAC patients compared to PNET (1154.74 U/ml vs. 217.44 U/ml) and older average age in PDAC patients compared to PNET (63 ± 23 years vs. 52 ± 34 years), reaffirming the tendency of malignant tumors to affect older individuals.

The pathophysiological bases supporting the differences in radiomic features between PDACs and PNETs are linked to their distinct biological behaviors. PDACs, characterized by hypovascularity and aggressive desmoplastic stroma, exhibit lower perfusion and higher heterogeneity in gray-level distributions, reflected in lower percentiles and increased entropy. Morover, it correlates with biomarkers like CA 19–9 and KRAS mutations, which drive its aggressive, poorly perfused phenotype. In contrast, PNETs, with their hypervascular nature driven by VEGF and VEGFR overexpression, is captured by high enhancement (e.g., ART_-firstorder_90Percentile, AUC 0.896), uniformity and well-circumscribed margins, show higher perfusion indices and more uniform texture features, particularly in the arterial phase, as evidenced by the elevated 90th percentiles and RootMeanSquared values. These radiomic signatures proxy microvascular density and perfusion differences, with PDAC showing sparse, dysfunctional vasculature and PNET displaying dense, functional vessels, offering potential for personalized diagnostics and therapy selection, such as anti-angiogenic treatments for PNET.

This study has some limitations. Firstly, the retrospective design of the study may have introduced potential bias. Secondly, lesion segmentation was performed manually by a single individual, and thus segmentation is inevitably influenced by inter- and intra-observer reproducibility. Such variability could affect the accuracy of radiomic feature extraction, particularly for texture parameters sensitive to boundary definition, potentially leading to systematic errors in distinguishing PDAC from PNET. Future studies could benefit from semi-automated segmentation tools or multi-observer approaches to enhance reproducibility. Additionally, the lack of standardized protocols across imaging platforms underscores the need for harmonization techniques, to minimize variability. Lastly, some subgroups of the study population do not represent a real sample of the population and are sometimes unbalanced, which could affect certain results.

5. Conclusions

Texture analysis of pancreatic pathology has shown good predictiveness in defining the PNET histotype. Radiomics may represent a supportive tool in diagnostic imaging for the differential diagnosis with PDAC, deserving further investigation and research to be validated.

CRediT authorship contribution statement

De Robertis Riccardo: Writing – original draft, Supervision, Methodology. **D'Onofrio Mirko:** Writing – review & editing, Validation, Supervision. **Cardobi Nicolò:** Writing – original draft, Supervision. **Spoto Flavio:** Writing – original draft, Methodology. **Bardhi Eda:** Writing – original draft, Data curation, Conceptualization. **Mascarin Beatrice:** Writing – original draft.

Declaration of Competing Interest

The authors declare that they have no known competing financial interests or personal relationships that could have appeared to influence the work reported in this paper. This study was conducted independently, and no external funding was received to support the research. All authors have approved the final manuscript and agree with its submission to European Journal of Radiology Open.

References

[1] M.J. Raphael, D.L. Chan, C. Law, and S. Singh, Principles of diagnosis and management of neuroendocrine tumours, Mar. 13, 2017, Canadian Medical Association. doi: 10.1503/cmaj.160771.

[2] M. Capasso, et al., Epidemiology and risk factors of pancreatic cancer, Mattioli 1885 (2018), https://doi.org/10.23750/abm.v89i9-S.7923.

[3] A.Z. Rogowska, Ultrasound-guided percutaneous core-needle biopsy of focal pancreatic lesions – practical aspectss, Pol. Ultrasound Soc. (2022), https://doi.org/10.15557/JoU.2022.0019.

[4] G. Chiti et al., Imaging of pancreatic neuroendocrine neoplasms, Sep. 01, 2021, MDPI. doi: 10.3390/ijerph18178895.

[5] M.E. Mayerhoefer, et al., Introduction to radiomics, J. Nucl. Med. 61 (4) (2020) 488–495, https://doi.org/10.2967/JNUMED.118.222893.

[6] B.A. Varghese, S.Y. Cen, D.H. Hwang, and V.A. Duddalwar, Texture analysis of imaging: What radiologists need to know, Mar. 01, 2019, American Roentgen Ray Society. doi: 10.2214/AJR.18.20624.

[7] B. Koçak, E.Ş. Durmaz, E. Ateş, and Ö. Kılıçkesmez, Radiomics with artificial intelligence: a practical guide for beginners, Nov. 01, 2019, AVES. doi: 10.5152/dir.2019.19321.

[8] M.G. Lubner, A.D. Smith, K. Sandrasegaran, D.V. Sahani, and P.J. Pickhardt, CT texture analysis: Definitions, applications, biologic correlates, and challenges, 2017, Radiological Society of North America Inc. doi: 10.1148/rg.2017170056.

[9] M.E. Mayerhoefer, et al., Introduction to radiomics, J. Nucl. Med. 61 (4) (2020) 488–495, https://doi.org/10.2967/JNUMED.118.222893.

[10] R.T.H.M. Larue, G. Defraene, D. De Ruysscher, P. Lambin, and W. Van Elmpt, "Quantitative radiomics studies for tissue characterization: a review of technology and methodological procedures, 2017, British Institute of Radiology. doi: 10.1259/bjr.20160665.

[11] A.M. Awe, V.R. Rendell, M.G. Lubner, and E.R. Winslow, Texture Analysis: An Emerging Clinical Tool for Pancreatic Lesions," Mar. 01, 2020, Lippincott Williams and Wilkins. doi: 10.1097/MPA.0000000000001495.

[12] P.T. Chen, et al., Radiomic features at ct can distinguish pancreatic cancer from noncancerous pancreas, Radio. Imaging Cancer 3 (4) (2021), https://doi.org/10.1148/rycan.2021210010.

[13] A. Zwanenburg, et al., The image biomarker standardization initiative: standardized quantitative radiomics for high-throughput image-based phenotyping, Radiology 295 (2) (2020) 328–338, https://doi.org/10.1148/radiol.2020191145.

[14] B. Ganeshan, et al., Non-small cell lung cancer: histopathologic correlates for texture parameters at CT 1, radiology.rsna.org n Radiol. 266 (1) (2013), https://doi.org/10.1148/radiol.12112428/-/DC1.

[15] B. Ganeshan, K. Skogen, I. Pressney, D. Coutroubis, K. Miles, Tumour heterogeneity in oesophageal cancer assessed by CT texture analysis: preliminary evidence of an association with tumour metabolism, stage, and survival, Clin. Radio. 67 (2) (2012) 157–164, https://doi.org/10.1016/j.crad.2011.08.012.

[16] K.A. Miles, B. Ganeshan, M.R. Griffiths, R.C.D. Young, C.R. Chatwin, Colorectal cancer: texture analysis of portal phase hepatic CT images as a potential marker of survival, Radiology 250 (2) (2009) 444–452, https://doi.org/10.1148/radiol.2502071879.

[17] R. De Robertis, et al., Liver metastases in pancreatic ductal adenocarcinoma: a predictive model based on CT texture analysis, Radiol. Med. 127 (10) (2022) 1079–1084, https://doi.org/10.1007/s11547-022-01548-8.

[18] C. Casà et al., The impact of radiomics in diagnosis and staging of pancreatic cancer, Mar. 01, 2022, SAGE Publications Ltd. doi: 10.1177/26317745221081596.

[19] M. D'Onofrio, et al., CT simplified radiomic approach to assess the metastatic ductal adenocarcinoma of the pancreas, Cancers (Basel) 13 (8) (2021), https://doi.org/10.3390/cancers13081843.

[20] "s00261–020-02833–8"

[21] M. D'Onofrio, et al., CT enhancement and 3D texture analysis of pancreatic neuroendocrine neoplasms, Sci. Rep. 9 (1) (2019), https://doi.org/10.1038/s41598-018-38459-6.

[22] J. Li, et al., Differentiation of atypical pancreatic neuroendocrine tumors from pancreatic ductal adenocarcinomas: Using whole-tumor CT texture analysis as quantitative biomarkers, Cancer Med. 7 (10) (2018) 4924–4931, https://doi.org/10.1002/cam4.1746.

[23] C.P. Reinert, K. Baumgartner, T. Hepp, M. Bitzer, M. Horger, Complementary role of computed tomography texture analysis for differentiation of pancreatic ductal adenocarcinoma from pancreatic neuroendocrine tumors in the portal-venous enhancement phase, Abdom. Radiol. 45 (3) (2020) 750–758, https://doi.org/10.1007/s00261-020-02406-9.

[24] S. Ren, et al., Differentiation of hypovascular pancreatic neuroendocrine tumors from pancreatic ductal adenocarcinoma using contrast-enhanced computed tomography, PLoS One 14 (2) (2019), https://doi.org/10.1371/journal.pone.0211566.

[25] T. Zhang, et al., Radiomics Combined with Multiple Machine Learning Algorithms in Differentiating Pancreatic Ductal Adenocarcinoma from Pancreatic Neuroendocrine Tumor: More Hands Produce a Stronger Flame, J. Clin. Med. 11 (22) (2022), https://doi.org/10.3390/jcm11226789.